Chasing charge localization and chemical reactivity following photoionization in liquid water

Ondrej Marsalek,[a] Christopher G. Elles,[b%] Piotr A. Pieniazek,[b&] Eva Pluhařová,[a] Joost VandeVondele,[c*] Stephen E. Bradforth,[b*] and Pavel Jungwirth[a*]

[a]*Institute of Organic Chemistry and Biochemistry, Academy of Sciences of the Czech Republic and Center for Biomolecules and Complex Molecular Systems, Flemingovo nám. 2, 16610 Prague 6, Czech Republic,* [b]*Department of Chemistry, University of Southern California, Los Angeles, California 90089-0482, USA* [c]*Physical Chemistry Institute, Zürich University, Winterthurerstrasse 190, CH-8057 Zürich, Switzerland*

*Corresponding authors: joost.vandevondele@pci.uzh.ch (J.V.), stephen.bradforth@usc.edu (S.E.B.), and pavel.jungwirth@uochb.cas.cz (P.J.)

[%]Present address: Department of Chemistry, University of Kansas, Lawrence, KS 66045, USA.

[&]Present address: Department of Chemistry, University of Wisconsin – Madison, 1101 University Avenue, Madison, WI 53706-1322, USA.

Abstract

The ultrafast dynamics of the cationic hole formed in bulk liquid water following ionization is investigated by ab initio molecular dynamics simulations and an experimentally accessible

signature is suggested that might be tracked by femtosecond pump-probe spectroscopy. This is one of the fastest fundamental processes occurring in radiation-induced chemistry in aqueous systems and biological tissue. However, unlike the excess electron formed in the same process, the nature and time evolution of the cationic hole has been hitherto little studied. Simulations show that an initially partially delocalized cationic hole localizes within ~30 fs after which proton transfer to a neighboring water molecule proceeds practically immediately, leading to formation of the OH radical and the hydronium cation in a reaction which can be formally written as $H_2O^+ + H_2O \rightarrow OH + H_3O^+$. The exact amount of initial spin delocalization is, however, somewhat method dependent, being realistically described by approximate density functional theory methods corrected for the self-interaction error. Localization, and then the evolving separation of spin and charge, changes the electronic structure of the radical center. This is manifested in the spectrum of electronic excitations which is calculated for the ensemble of ab initio molecular dynamics trajectories using a QM/MM formalism applying the EOM-IP-CCSD method to the radical core. A clear spectroscopic signature is predicted by the theoretical model: as the hole transforms into a hydroxyl radical, a transient electronic absorption in the visible shifts to the blue, growing toward the near ultraviolet. Experimental evidence for this primary radiation-induced process is sought using femtosecond photoionization of liquid water excited with two photons at 11 eV. Transient absorption measurements carried out with ~40 fs time resolution and broadband spectral probing across the near-UV and visible are presented and direct comparisons with the theoretical simulations are made. Within the sensitivity and time resolution of the current measurement, a matching spectral signature is not detected. This result is used to place an upper limit on the absorption strength and/or lifetime of the localized $H_2O^+_{(aq)}$ species.

Introduction

The radiation chemistry of pure water initiated by ionization leads to formation of an excess electron which leaves behind a cationic hole.[1] Each of these two charged radical species formed by ionizing radiation follows its own route of chemical reactivity. On one hand, H_2O^+ is an extremely unstable radical cation which reacts with a neighboring water molecule by proton transfer, forming the H_3O^+ cation and the OH radical. The latter species is involved in further oxidative processes.[1] On the other hand, the excess electron relaxes to a localized solvated electron, which can go on to reduce impurities such as ions, free radicals, or dissolved oxygen on the sub-microsecond timescale.[1-4] Even in pure water, the solvated electron can react with other hydronium ions, other solvated electrons formed in the spur and with water itself which results in an inherent lifetime which does not exceed several miliseconds.[1,5-7] How far away the solvated electron localizes determines the yield of these strongly oxidizing and reducing radicals available for subsequent chemistry. If trapped close by (< 3 nm), the electron may recombine back with either the OH radical or H_3O^+ at the hole site. The preferred geminate recombination partner and the kinetics of recombination is in turn be governed by the precise interaction and correlation of the motions of the H_3O^+ and OH pair formed in the primary proton transfer step.[8,9] For the brief period before full solvation, the electron exhibits enhanced reactivity and this has been suggested to also affect the recombination yield and the production of H_2.[10]

The products of ionization of water, in particular the OH radical are important species involved in the indirect radiation damage of materials and biomolecules including DNA.[11] Therefore, numerous kinetic studies have been devoted to elucidating the rates of processes induced by water ionization.[12] At ultrafast times and at the molecular level, unlike for the

solvated electron product, the information about the chemical dynamics of the cationic hole leading to formation of OH is not so clear and subject to far fewer investigations.[8,9] It is usually assumed that the proton transfer reaction happens faster than 100 fs and this value is given in nearly all introductory texts on radiation damage of water and biological tissues.[13] This number derives from a pioneering photoionization study soon after the availability of amplified sub-picosecond pulses when an attempt was made to capture this primary step in the radiation chemistry of water. Gauduel and his co-workers claimed detection of H_2O^+ and its decay time, measured as 100 fs (and 170 fs in D_2O), through transient absorption.[14] Their experiment used photolysis at 8 eV, but recent experimental evidence[15] and theoretical insight into the electronic structure of water indicates that 8 eV is not in fact sufficient to generate the H_2O^+ cation directly, and that the mechanism for ionization at this energy involves hydrogen atom motion in the excited state neutral water molecule to reach a solvated electron.[16-18] For such ionization pathways around 8eV, it is now understood that H_2O^+ cannot be an intermediate and photodissociation dominates. The interpretation of the origin of signals in ref. [14] is discussed later. Regardless, the important questions remain about over what timescale the proton transfer reaction happens and what electronic signature would be expected for the turnover of H_2O^+ into OH.

On the computational side, quantum chemical methods have recently[19-23] been employed to map the potential energy surface, dynamics, and spectroscopic properties of the simplest cluster model – the water dimer cation. These studies all show it is essentially a barrierless process for the system to convert from H_2O^+ ...H_2O to H_3O^+ ...OH after removal of the electron. Based on the shape of the potential surface it was suggested that starting from the optimal geometry of the neutral water dimer, the distance between the oxygens of the two water

molecules decreases upon ionization from 2.9 to 2.5, after which a proton hops from H_2O^+ to H_2O forming the above products.[20] A more recent work following the dynamics using quantum mechanical wave packet propagation reveals that the proton can oscillate between the two oxygens several times as the waters come closer together but the reaction is essentially complete in 50 fs.[23] In both papers, it is predicted that these chemical changes are accompanied by shifts in the electronic spectrum, which is in principle accessible to ultrafast UV/visible transient absorption spectroscopy. In subsequent studies, ionization was modeled in larger clusters with up to five water molecules, which allowed investigation in a limited sense, i.e., for small systems, of the character of the charge delocalization upon ionization.[24-26] A partial delocalization (which is not present in the ionized water dimer, where the charge is initially fully localized on the hydrogen bond donating water molecule) was observed in these small water clusters.[25] Additionally, an ab initio molecular dynamics study of ionization in a cluster with 17 water molecules was performed recently which, however, due to the use of the Hartree-Fock method leads to a localized charge already at the instant of ionization.[27]

The previously studied ionized water clusters allow investigation of the onset of the medium effects, nevertheless, they are still very far from the condensed phase. A natural question therefore arises as to what is the degree of charge delocalization upon ionization in liquid water (i.e., what is the nature of the nascent bulk "H_2O^+") and whether this delocalization can play a role in slowing reaction from the cationic hole toward H_3O^+ and OH products in the aqueous bulk. To address this issue we have employed ab initio molecular dynamics (AIMD) simulations of ionization in bulk water by removing the least bound electron. Dynamics following vertical ionization to the lowest ionized state was followed on the 1 ps timescale, which was sufficient to observe both hole localization and chemical reactivity. As with the

water dimer cation studies, we correlate the changing electronic structure of the radical cation as its structure evolves along the reaction coordinate with the changes in the electronic absorption spectrum computed with the EOM-IP-CCSD method. A clear spectral evolution is predicted as the system moves toward the OH product.

These encouraging theoretical predictions suggest that a renewed attempt at experimental measurement of the lifetime of H_2O^+ in liquid water is warranted, particularly as factor of ~3 times higher time resolution and full broadband probing is now possible compared to earlier experiments.[14] Such experiments would provide an important benchmark for verifying the AIMD spin localization and proton transfer dynamics. The short-lived water cation is still an extremely experimentally challenging target, in part because the spectroscopic signature of hydrated H_2O^+ remains a theoretical prediction that has never been experimentally observed in clusters or the bulk. Additionally, the timescales predicted for the proton transfer reaction are still right at the current state of the art in ultrafast time resolution, and a relatively weak electronic absorption is expected for H_2O^+ compared to absorption in the electron channel. Despite these concerns, a new experimental search to detect the initial hole and its evolution into OH is reported here. Our approach is to photoionize at energies where we expect strong coupling to the ionization continuum; the H_2O^+ species can be expected to be formed at a high quantum yield by two-photon excitation of bulk water once sufficiently high photolysis energies are used.[16] Recent studies from Crowell and Bradforth groups suggest that excitation near 11 eV strongly favors ionization over the competing dissociation channel,[28] and 11 eV is near the vertical ionization potential of liquid water corresponding to the first $1b_1^{-1}$ ionization continuum.[16,29] However, we should bear in mind the fact that the absorption spectrum of liquid water at these energies is dominated by several electronic resonance states which means that

ionization might either take place to the $1b_1^{-1}$ continuum or possibly by autoionization into the next higher ionization continuum, the $3a_1^{-1}$.[30,31] Based on our current assignment of the two-photon absorption spectroscopy,[31] we expect the formation of a $1b_1^{-1}$ hole to be the most likely outcome following two-photon excitation at 11 eV with H_2O^+ formed within the pulse duration.

One other complication for a direct comparison of theory and experiment is that ab initio MD follows the dynamics of the lowest state of the system after removal of the least bound electron of the whole system. At the neutral geometry, there is a plethora of low-lying (excited) states of the cationic systems forming the quasi-continuous $1b_1^{-1}$ band. In the experiment, the intra-band relaxation also contributes to the localization process. To describe this part of the process one would need to perform non-adiabatic dynamics involving many electronic states, a calculation beyond those currently feasible within the all electron description.

In the following we start by describing the ab initio molecular dynamics methodology for modeling the ultrafast chemical dynamics of the cationic hole in water and the QM/MM coupled cluster calculations used to simulate the corresponding time-evolving electronic absorption spectra. Then we describe AIMD results for the localization and proton transfer dynamics of the cationic hole, benchmarked against highly accurate ab initio calculations for small water clusters. Simulations of the time-dependent electronic spectrum using the structural configurations from the AIMD trajectories are then presented, illustrating how they can be used to track the evolving reaction dynamics. The key spectral signature of the reaction $H_2O^+ + H_2O \rightarrow OH + H_3O^+$ is a blue shift of an absorption line from about 2.5 to 4eV, corresponding to a conversion of a localized cationic hole to the OH radical. Finally, an attempt to experimentally monitor the transient spectroscopy initiated after photoionization is described with time resolution and probe

spectral range such that a one-to-one comparison with the simulations is possible. The experimental result is used to bracket possible outcomes of the reaction dynamics in the system.

Methods

We performed Born-Oppenheimer dynamics simulations of a cationic hole in a periodic box of 64 or 128 water molecules. Forces and energies were calculated from Kohn-Sham density functional theory (DFT), using functionals of the generalized gradient (GGA) approximation type (BLYP or PBE) and, for several trajectories, including an empirical dispersion correction (BLYP-D).[38] The canonical (NVT) ensemble was simulated, with the volume based on experimental water density and the temperature set to T=350 K for pure GGA DFT and T=300 K for BLYP-D. The hybrid Gaussians and plane waves scheme was used with a TZV2P basis set for the Kohn-Sham orbitals and a 280 Ry cutoff for the auxiliary plane wave basis set.

After equilibration of a neutral water system, snapshots from a further trajectory separated by 500 fs were taken as different initial conditions for simulations of the dynamics following ionization. To this end, one electron was removed by changing the total charge of the system at t = 0 to model vertical ionization of the system. Since this procedure leads to an open shell system, the self-interaction correction (SIC) was used for the singly-occupied orbital in a restricted open-shell formulation of the Kohn-Sham equations. The SIC parameters a=0.2 and b=0 were tested previously for the solvated OH radical,[39] as well as for the water dimer cation, yielding results comparable to highly accurate wavefunction-based methods.[20,21]

For comparison, further calculations (both single-point energy evaluations and test dynamical runs), were performed with the HSE hybrid functional,[40] the ``half-and-half" hybrid functional,[41] and, for the sake of completeness, also with pure Hartree-Fock exchange (HFX). As shown

previously,[42] the admixture of a significant fraction of exact exchange in the density functional can improve the description of cationic radical systems. The optimal fraction of exchange is system dependent and, for example, the BH&HLYP functional contains 50% HFX, while the more common B3LYP functional only contains 20% HFX. For the condensed phase, functionals that employ screened exchange have a computational advantage.[40,42] In the present notation, e.g., HSE(0.5) refers to the HSE functional in which the fraction of exchange is 50%. Additional benchmark single-point calculations were also performed on a small cluster of five water molecules for comparison with available results calculated using the very accurate EOM-IP-CCSD method.[25,43] The DFT calculations for the cluster were set analogously to the bulk calculations, except that open boundary conditions were used. All ab initio molecular dynamics simulations were performed using the CP2K package and its DFT module Quickstep.[44]

Spectral calculations using EOM-IP-CCSD/6-311++G** focused on the excited states of a reactive sub-system (*vide infra*) below 6 eV excitation energy. Such a high level of theory is necessary to properly describe the excitation energies and the associated transition properties.[20] However, at the coupled cluster level only a small core of the molecular system can be included quantum mechanically. Excitations lower than 6 eV will only originate from the open shell part of the system, so such a division of the system into a QM and MM part is only meaningful once the spin has partially localized. Our model defines a reactive trimer core by (i) the oxygen atom of the water molecule that transfers the proton, (ii) two oxygen atoms closest to the hydrogens of the proton transfering molecule. Hydrogen atoms are included in the trimer if they are less than 1.5 Å from either of the oxygens. We chose a trimer, rather than a dimer, as our basic quantum mechanical core as in the molecular dynamics we observed several large amplitude vibrations of either OH bond in the central water molecule, before the actual reactive step takes place. Further,

dynamically defining the trimer allowed to account for subsequent proton hops (from H_3O^+ to neighboring H_2O). Static selection of the oxygen trimer framework is justified by the long time scale of water diffusion. Thus, in effect quantum mechanical calculations were performed either on $(H_2O)_3^+$ or $OH(H_2O)_2$, with the remaining water molecules treated as point charges taken from the SPC/E water model (-0.8476 and 0.4238 for oxygen and hydrogen, respectively).[45] Each trajectory was followed up to 500 fs. Along each trajectory, the EOM-IP-CCSD excitation energies werer computed based on the closed-shell reference. In order to construct transient absoprtion spectra at each step a 0.6 eV FWHM Gaussian was applied to each transition. Experimental linewidths in electronic spectra of related systems such the spectra of OH(aq) and H_2O itself are 1 eV or greater,[31,43,46] due to the extremely strong solute-water coupling and so this rather arbitrary choice of width is likely an underestimate. Essentially, the inclusion of additional broadening is necessary because of under-sampling of the distribution of liquid structures, assuming inhomogeneity is the major determinant of the lineshape. The calculations using wavefunction-based methods were performed using the Q-CHEM program.[47]

Results and Discussion

Ab initio MD following photoionization in bulk water

We simulated over 20 trajectories following ionization of bulk water, started with different initial conditions. To this end we employed the BLYP-SIC functional with the self-interaction correction optimized against accurate Coupled Cluster calculations for the water dimer cation. For illustration, Figure 1 depicts three crucial snapshots from a representative trajectory. The first snapshot shows the cationic hole right after photoionization, i.e., with nuclei in the geometry of neutral water. We see that the spin density of the cationic hole is delocalized over several

water molecules (a detailed discussion about which water mlecules are most prone to carry the spin initially is presented in the Supplementary Material and in Refs. 48-50). However, the hole localizes very fast on a single water molecule (second snapshot in Figure 1). Such a localized H_2O^+ moiety becomes extremely reactive, forming H_3O^+ and OH in a reaction with a neighboring water molecule, as depicted on the third snapshot in Figure 1. The products are first formed as a contact pair, but later become separated by one or more solvent molecules due to proton hops from the originally formed hydronium moiety to neighboring waters.

For further description of the ultrafast dynamics of the cationic hole and in order to draw robust conclusions we now provide data for the whole set of simulated trajectories. Figure 2 shows the time evolution of the largest Mulliken spin population found on an oxygen of a water molecule for all trajectories. At the instant of photoionization, this largest spin density amounts to 0.1-0.3, indicating significant spin delocalization over several water molecules (*vide infra*). However, with a mean time of 31 fs (with a mean deviation of 21 fs) 95 % of the spin localizes on a single water molecule (see Table 1). The progress of the chemical reaction toward H_3O^+ and OH is then monitored in Figure 3, which depicts for all trajectories the time evolution of the distance between the center of spin and the center of charge. During the localization process and before the reaction both spin and charge localize on a single water molecule forming H_2O^+, therefore this distance equals to zero. Right after the reaction, which proceeds as a proton hop from H_2O^+ to a neighboring water molecule, charge (H_3O^+) and spin (OH) become separated by a short hydrogen bond of about 2.6 Å. The first proton hop occurs on average at 33 fs (with a mean deviation of 14 fs), which practically coincides with the 95 % localization time (Table 1). However, for many trajectories re-crossings back to reactants take place with the final stabilization of the products occurring on average 44 fs after the first proton transfer. Afterwards,

the proton can hop to other water molecules and the products become separated by a larger distance with most of the H_3O^+ ...OH contact pairs disappearing within 200 fs (Figure 3). It is likely that due to the classical treatment of all nuclei the proton transfer time and the number of re-crossings are somewhat overestimated in the present calculations, which thus likely present a lower bound to the proton transfer rate.[51]

It is useful to combine the principal results presented in Figures 2 and 3 into a single picture (Figure 4), which correlates for each trajectory the localization time with the moment of occurrence of the first proton transfer. We clearly see from Figure 4 that the first proton transfer proceeds at the instant of, or right after, the spin localization, with the reaction being over (i.e., no more re-crossings occurring, open circles) for most trajectories several tens of femtoseconds later. Another useful correlation for understanding the process is that of the distance between the oxygen atoms involved in the proton transfer reaction with the distance between the transferring hydrogen atom and its new oxygen binding partner. This correlation is plotted for all simulated trajectories in Figure 5. We see that in the initial stages of the reaction both distances shrink simultaneously (blue segments in Figure 5). Also, the shorter the initial O-O distance the faster the system reaches the region where proton transfer starts occuring. Between the first proton hop and the time when the recrossings cease to occur the two oxygens stay close to each other (red segments). Once the two oxygens separate by more than 2.7 Å, the reaction is essentialy over with the nascent H_3O^+ and OH products forming first a contact pair and later being separated by water molecules. Note, that the shape of the trajectories in Figure 5 corresponds to a potential energy surface which is remarkably similar to that of the water dimer cation,[20] indicating that after spin localization the reaction proceeds locally with $H_2O^+$and one or at most two other water molecules directly involved.

Benchmarking the initial delocalization of the cationic hole

The initial degree of spin delocalization of the cationic hole is, from the computational point of view, a subtle issue which is dependent on the electronic structure method employed, as demonstrated in Figure 6. The figure depicts, for a selected trajectory, the spin density in the unit cell of water right after ionization (t = 0), as obtained by different methods. As already discussed above, the BLYP-SIC functional yields a partially delocalized initial hole (Figure 6). The importance of the self-interaction correction emerges from comparison to the uncorrected BLYP results (Figure 6), which results in a spin density which is over-delocalized (*vide infra*). This over-delocalization is caused by the self-interaction error, leading to a spurious repulsion of the unpaired electron by itself.[42] The other extreme situation, i.e., complete localization of the initial cationic hole results from Hartree-Fock calculations (Figure 6), where the artificial overlocalization is due to a symmetry breaking problem.[51] Hybrid functionals to a large degree cancel out these two errors. Figures 6d,e show the initial spin density following from calculations with the HSE functional with 25 or 50 %[42] of exact exchange mixed in. While the first mixing value is similar to that used in most standard hybrid functionals, the second one matches best the Equation of Motion Coupled-Clusters (EOM-IP-CCSD(T)) energy of the water dimer cation.[20] In both cases we get a partially delocalized hole with its delocalization decreasing with increasing mixed-in fraction of exact exchange. The degree of initial delocalization from BLYP-SIC, employed in the dynamical calculations, is comparable to that obtained using the hybrid functional, being actually bracketed by the two HSE calculations. Further discussion of benchmarking along the dynamical trajectories is presented in the Supporting Material.

The fact that the structure and dynamics of the cationic hole in water sensitively depends on the approximations employed in the electronic structure calculations demonstrates the big challenges of the present problem and calls for benchmarking against a very accurate method such as the EOM-IP-CCSD.[20] Such calculation can only be performed for a small cluster model. We chose the smallest system with a tetrahedrally coordinated water molecule, i.e., the water pentamer cation in the geometry of a neutral cluster with one central water molecule hydrogen bonded to four others.[25] Figure 7 shows the spin densities after ionization of the neutral water pentamer using all the methods discussed here. The benchmark EOM-IP-CCSD spin density is partially delocalized over the two water molecules with no accepting hydrogen bonds. It is reassuring that the "workhorse" for the present study, i.e., the BLYP-SIC methods compares very well to EOM-IP-CCSD. The hybrid HSE functionals also perform satisfactorily, with HSE 25 % slightly overestimating and HSE 50 % slightly underestimating the spin delocalization. In contrast, BLYP over-delocalizes and HF over-localizes the initial spin density compared to the benchmark result.

Modeling of the absorption spectra

In order to facilitate connection to ultrafast electronic spectroscopy we have evaluated electronic spectra along the AIMD trajectories. In our earlier work,[20] we calculated the absorption of the water dimer cation at various geometries along the proton transfer coordinate and this provides a helpful starting point for the bulk liquid ionization. The dimer cation is the simplest model of the proton transfer reaction in bulk water, where fully ab initio high-level calculations of the absorption spectrum are tractable.[20] We found that at the geometry of the neutral water dimer, the dimer cation has a calculated absorption near 620 nm that is associated

with the H_2O^+ moiety and decays with the timescale of the proton transfer reaction. Following the reaction coordinate downhill to a weakly bound H_3O^+...OH pair, a calculated absorption band in the UV corresponds to a purely valence transition on the OH radical.[20] A similar evolution of the optical signature is found for the gas phase dimer cation with wave packet time dynamics computed explicitly.[23]

Here we have generalized this approach to follow the bulk AIMD trajectories presented above and tried to include as much of the effect of the extended solvent on the electronic excitations as possible. As discussed in the methods section, we have done this using a QM/MM approach. The reactive trimer is described by the EOM-IP-CCSD electronic structure method, while the rest of the system is described by point charges. While this limits the description of the delocalization, we can still follow how the reactive process influences the spectroscopy as the proton transfer reaction proceeds. In addition, we are sampling a range of initial H-bonding geometries in the liquid and structural changes of the network along the AIMD trajectories contain the collective effects of the liquid (e.g., "solvent drag") in modulating purely ballistic motions. In the AIMD simulations the hole is initially partially delocalized, whereas here, the forced localization from the very earliest times allows us to obtain a clear picture of the spectral signature of the localized hole and thus a means to disentangle the spectroscopy from the localization dynamics.

At early times (t= 0 - 30 fs) we observe a very strong absorption spanning the entire 1 – 5 eV energy range (Figure 8(a)). Very little nuclear dynamics has occurred up to this point, consequently the electronic states of all three water molecules are approximately degenerate. In particular, the configuration of the two hydrogen bond accepting molecules is conducive to the formation of an intense charge-resonance band.[25] Due to the absence of symmetry constraints

this transition couples to all the other excitations yielding intense bands throughout the entire spectral range. As the reaction proceeds, a close degeneracy between the two accepting molecules, one of which becomes H_3O^+, is lifted, the charge-resonance transition disappears, and lower intensity is observed throughout the entire spectrum.

Subsequently, as this broad absorption dies away, a new absorption band is seen, weak at first and rapidly blue shifting as it grows. By extrapolating to early times (more easily seen in Figure 8(b)), this feature starts at ~2.3 eV (540 nm) at 30 – 50 fs and evolves to ~ 4 eV (310 nm) by the end of the computed time window. The band is not fully developed in intensity until ~150 fs. We note that a rising, blue shifting band is similar to predictions for the dimer cation.[20,23] This evolving band has been assigned as the H-bond donor $a_1 \rightarrow b_1$ (or $(a_1/b_1)^*$ and $(a_1/b_1) \rightarrow (b_1/0)$ in the dimer molecular orbital formalism introduced in ref. [20]) transition at the vertical ionization geometry turning into the $\sigma \rightarrow \pi$ valence transition on OH with increased oscillator strength.[20] In the bulk simulation, the $a_1 \rightarrow b_1$ transition starting out near 2.3 eV, which we are assigning to localized H_2O^+, is considerably weaker than in the dimer work. There is one other noticeable difference in the time-evolving spectrum between the gas phase dimer and the bulk. In the wave packet simulations of Kamarchik et al., the proton is first transferred in ~10 fs and the spectral shift from 3 to 4 eV is over in 30 fs.[23] This suggests that the delayed onset of proton transfer events in the bulk simulations, brought about by a rate limiting localization step, is manifested by slower spectral shifting in the electronic spectra. The influence of the surrounding waters (included as point charges) seems to introduce only modest changes to the basic spectral features, for example slightly red shifting the terminal OH(*aq*) band compared to the gas phase dimer.

It is perhaps understandable that the current spectral predictions map so well to the dimer

cation spectra (with the exception of the timescales) because there is an artificial localization inherent to the present computational procedure. Although the nuclear motions are dictated by the full AIMD and proton transfer is inhibited until spin localization has taken place, the small size of the QM core (and particularly the fact we carve out a trimer with a central double H-bonded donor[25]) in the EOM-IP-CCSD calculations is prematurely forcing the electronic structure to localize in the spectral calculations. As we do not know what the spectral signature of an initial hole spread throughout the water network is, we turn on the spectra only after 95% localization is achieved for each individual DFT trajectory, where we expect the coupled cluster trimer to be a reasonable starting point for predicting the electronic spectrum (Figure 8b). This removes the strong initial feature, while the rest of the spectrum is not affected. Spectrally ignoring the first phase can be further justified when making a comparison to experiment as this temporal region is obscured by a separate coherent spectroscopic transition (*vide infra*) due to pulse overlap. This *ad hoc* procedure has the advantage of highlighting the weak early feature in the spectral simulations between 2 and 2.5 eV which we have assigned as the spectrum of the localized H_2O^+ hole. Clearly, an improved description of the electronic spectroscopy including a large quantum mechanical region is highly desirable to determine the spectroscopic signal of the early delocalized hole, but such an approach is beyond current computational capabilities.

Experimental search for the cationic hole and its evolution by femtosecond transient absorption

The ratio of the calculated oscillator strength at the proton-transferred geometry to the experimental[46] extinction coefficient of the OH_{aq} ($\sigma \rightarrow \pi$) transition in liquid water gives a scaling factor that can also be used to estimate the transition strength for a localized hole. Due to the uncertainties described in the preceding paragraph, we use for this estimate the earlier value[20,25]

for $(H_2O)_2^+$ at the vertical dimer cluster geometry. This crude analysis suggests an experimental extinction coefficient of at least 80-100 $M^{-1}cm^{-1}$ at peak for localized H_2O^+, equivalent to about 0.4% of the maximum absorptivity of the equilibrium solvated electron (and comparable to the OH radical valence band absorption near 310 nm) originating from the photoionization process.[52] Note that we make our comparison with the long wavelength part of the OH(aq) absorption that has been assigned to the valence transition rather than the stronger charge transfer component at wavelengths shorter than 300 nm. The experimental extinction coefficient at the maximum of the OH ($A \leftarrow X$) transition in water is ~125 $M^{-1}cm^{-1}$ at 350 ^oC, ref. 46, where hydrogen bonding is significantly reduced from room temperature, approximating the dimer. The calculated UV absorption band in the proton-transferred geometry of the dimer is ~1.5 - 1.7 times stronger than the calculated absorption of the cation dimer at the initial geometry.

The solvated electron absorption takes 2-3 ps to reach it maximum value due to trapping and relaxation dynamics,[16,53] leaving a potential window (despite this unfavorable detection contrast ratio) to probe the newly localized hole. Assuming then that ionization produces equal numbers of H_2O^+ and solvated electron, the estimated extinction coefficient puts the H_2O^+ absorbance very close to experimental detection limits in favorable cases where the solvated electron signal exceeds 20 mOD. In addition, a fraction of the electrons are likely to undergo geminate recombination during the 2-3 ps before the solvated electron signal reaches its maximum, suggesting a higher initial concentration of H_2O^+ than implied by the electron signal.[54] So, although the H_2O^+ absorption is almost certainly weak, the fact that it is quite possibly within our detection limits convinced us to attempt a search for the experimental signal in the transient absorption spectrum.

Broadband pump-probe measurements were therefore performed that probe the range from 300 to 800 nm. Our experimental apparatus has been described in detail previously.[16,17,31] Briefly, 30 fs pulses centered between 223 – 227 nm derived from four-wave mixing in a hollow-core fiber[55] are focused into a 70 μm thin flowing film of neat liquid water.[56] At the focus, two-photon absorption of the pump by water leads to prompt ionization, and a broadband white light continuum brought to a narrower focus probes the absorption of products. The differential absorption from the continuum is measured on a photodiode array with the pump blocked every other shot. Figure 9 (A, C) shows two datasets covering different parts of the continuum probe transient absorption spectrum. A strong two-photon (pump + probe) absorption at short wavelengths dominates the signal near time-zero, where the pump and probe pulses overlap in time,[31] while the absorption at longer wavelengths rises with a timescale of ~1-2 ps due to the formation of solvated electrons[57,58] neither of which is accounted for in the present AIMD simulations. Although well understood, these two strong features complicate the search for a weak transient absorption by a localized H_2O^+. As shown in the representations of the computed spectrum in the panels B and D of the figure, the H_2O^+ species is expected to absorb from 600 – 500 nm, with a lifetime determined by the proton-transfer reaction, and then evolve into an OH radical that absorbs in the near-UV (most clearly seen in panel B). Comparing panels A with B and C with D in Figure 9, as well as their cuts (Figure 10), shows that there is no clear experimental signature for a localized H_2O^+ which would appear sandwiched between these two other intense features in the dispersed 2D dataset. From comparing panels A and B, it is clear that even the signal from the final product OH radical (expected with intensity ~ 0.2 – 0.3 mOD is itself difficult to discern above the continuous tail of the rising electron band, surprisingly already present at short wavelengths just after the 30 fs ionization pulse). Figures S3 and S4 in

the Supporting Information show additional data and the OH spectral band contribution expected (based on that detected from H_2O_2 photolysis).

Careful examination of the pump-probe anisotropy and power dependence of the signal do not reveal any sign of a spectroscopic signature of H_2O^+. Weak absorption by the short-lived H_2O^+ transient species is the most likely explanation for the absence of an experimental signal. Another possible experimental limitation is the short lifetime of the H_2O^+ species, because the strong two-photon absorption peak dominates the transient spectrum up to about 40 fs. This experimental complication means that regardless of our uncertainty in the spectral signature prior to localization (and omitted in Figure 8(b) and Fig 9(A and C)), the experiment won't be able to comment on the spectral evolution during this earliest period. The best case experimental time-resolution of ~40 fs is determined by the duration of the pump laser pulse; this limits our observation window to transient species with lifetimes longer than about 30-40 fs. Cross-phase modulation and non-linear dispersion of the broadband probe pulses further complicate the signal at very short delay. This can be seen in the data in panel A using continuum light generated at 800 nm; we obtained better time resolution and stronger signal using this continuum but significant cross phase modulation artifacts (marked on plot with arrow) can be seen in this data which complicate its interpretation. The data in panel C were recorded using broadband probe light generated at a central wavelength of 1350 nm, where the cross-phase modulation and dispersion effects are minimal. Overall, analysis of all of our data suggests we find no evidence for H_2O^+, including where the time resolution is as short as 40 fs and where the solvated electron signal exceeds the target 20 mOD. Although our experiments fail to reveal a signature we can associate with a H_2O^+ species, based on our experiments we can rule out the previous measurement of Gauduel as an observation of H_2O^+ or its reported lifetime.[14] We have also been

able to place limits on the cross section and/or the lifetime of this species.

The earlier[14] pump-probe experiments delivered 8 eV of energy into water, as compared to 11 eV employed here. As remarked on in the Introduction, we now know that two-photon photolysis of water near 11 eV yields a much higher fraction of ionization events (compared to dissociation events) than two-photon excitation at 8 eV[28,59 59]and at much lower pump intensity due to the much higher 2PA cross section.[31] In that case, if the proton transfer reaction timescale was 100 fs, the decaying signal assigned to H_2O^+ by Gauduel near 400 nm probe would then be readily seen here (Figure 9(A)) with shorter pulses and at 11 eV total excitation energy. The signal in ref. [14] instead of being due to H_2O^+ is most likely due to simultaneous absorption of one pump and one probe photon when the two laser pulses are overlapped in time.[31] No excited state is formed in this pathway and the width of the feature is instead determined by the cross correlation of the two pulses. If any of the signal is due to population formed by absorption of two pump photons (no intensity dependent data is given in ref. [14]), this part of the signal must originate from absorption from the excited state of neutral H_2O and the free[4346] OH radicals formed via very rapidly by direct dissociation.[28] Preliminary measurements in our lab show rotationally hot OH radicals, formed in greater yield by photodissociating H_2O_2 than two-photon water photolysis, absorbing out to 400 nm (Figure S4).[60] We reiterate that H_2O^+ is not formed with 8 eV total energy deposition.

If the lifetime of H_2O^+ is as short as the current AIMD trajectories indicate, more intense pump pulses would increase the likelihood of observing the proton-transfer reaction directly. Shorter pulses give better time-resolution but at the expense of increased cross-phase modulation artifacts. More intense pulses would increase the population of H_2O^+ (quadratic in pump intensity) and thus the signal relative to the 2PA feature which is linear in the pump. However, if

(as indicated by AIMD calculations) the initial cationic hole is delocalized and upon localization reacts fast, this means the population of the localized H_2O^+ will be small at any time, and that even shorter pulses may not resolve the problem of its detection.

There are some additional factors we should consider. In the calculations we have made an assumption that H_2O^+ is formed in its ground electronic state, since excited state dynamics would involve calculations of the higher states and non-adiabatic couplings, which are both highly non-trivial tasks in the condensed phase. It is possible that it is also non-trivial experimentally to produce a ground state H_2O^+. It may be that in the experiment ionization at 11 eV does not exclusively lead to H_2O^+ with a $(1b_1)^{-1}$ hole and consideration of the excited resonance state of water prepared would then be necessary.[31,61] In this scenario, excitation would promote an electron from the second highest occupied orbital, $3a_1$ (just as in the gas phase $\tilde{B} \leftarrow \tilde{X}$ band) and this is more likely to autoionize to give an excited state $(3a_1)^{-1}$ cation, or decay through a neutral dissociative mechanism that does not produce H_2O^+ as a transient. The dynamics subsequent to ejection of a $3a_1$ electron from the water dimer has recently been considered by Kamarchik et al.[23] The excited H_2O^+ cation so formed is metastable to proton transfer, and also has a very different excited state spectrum compared to the ground state localized cation here so far considered. The dissociation scenario is analogous to the neutral pathway that we have previously indicated plays a role at lower excitation energies near 8 eV, except that OH radicals will be formed in an electronically excited state. Therefore, neither of these putative $3a_1$ promotion channels produce the ground state H_2O^+ we have sought here. The relative two-photon cross-sections for the various $(1b_1)^{-1}$ and $(3a_1)^{-1}$ excited states and also for direct ionization determine the importance of each of these channels. Despite this possible explanation for the non-observation of ground state H_2O^+ signal, our current assignment of the

liquid water spectrum still suggests that at 11 eV transitions to $(1b_1)^{-1}$ dominates over any $(3a_1)^{-1}$ excitation pathway.[31]

Conclusions

We have investigated in detail the reaction dynamics of the cationic hole formed in water after ionization by high energy radiation. Not only is this reaction of fundamental importance in radiation chemistry but this is an excellent test case for ab initio molecular dynamics, complementing the numerous studies that have considered the excess electron in water. We find that from a theoretical perspective, there is an initially partially delocalized state and that the localization transition is of key importance in determining the overall timescale for the reaction process. The degree of delocalization and the timescale for localization however are critically determined by the amount of HF exchange included in the DFT treatment. We have carefully benchmarked a self-interaction correction for BLYP against varying amounts of exact HF exchange and EOM-IP-CCSD for small clusters.[20,25,62] For such a benchmarked DFT model, the average localization time is ~ 30 fs and proton transfer starts practically immediately. Although the proton transfer step may proceed even faster if quantum tunneling is accounted for, as localization is found to be rate limiting here, tunneling should not influence the overall kinetics.

Simulated electronic spectra are constructed using a QM/MM scheme based EOM-IP-CCSD and the structural snapshots from the set of AIMD trajectories. These predict an electronic signature shifting across the visible into the near-ultraviolet and intensifying with time that provides a means to track the reaction $H_2O^+ + H_2O \rightarrow OH + H_3O^+$. A transient absorption experiment with 40 fs time resolution was carried out but did not see any such signature of reaction in the visible and near UV. The spectral simulations make clear that determining a

reaction time by monitoring transient absorbance in the ultraviolet (in the stronger charge transfer part of the OH spectrum[43]) is not an unambiguous marker for the appearance time, as the system absorbs in this region even prior to proton transfer. This experimental result definitively overturns the prior value of 100 fs based on pump-probe spectroscopy and very often quoted in the literature and introductory texts on radiation chemistry for this reaction.

Several points concerning the experiment should be acknowledged: (i) Our sensitivity to a localized H_2O^+ based on its visible band oscillator strength may not be sufficient. (ii) Because the localization step is rate-limiting for the overall reaction, the localized H_2O^+ starts reacting immediately and so is never strongly populated. This, together with the distribution of the starting times of the reaction (equivalent to the localization times) makes it difficult for the experiment to detect. (iii) In the experiment, due to complexities of the photoionization process itself which are yet to be fully understood, the system may not start out on the ground state cation surface considered by AIMD. (iv) It is possible that the reaction time is indeed at the lower limit of the theoretical prediction and is, therefore, not resolvable with current temporal resolution of the experiment.

In summary, we have characterized the ultrafast dynamics following photoionization in bulk water with AIMD simulations. These calculations provide a detailed molecular picture of the cationic hole localization and subsequent proton transfer and a <40 fs timescale for the overall reaction is consistent, but not proven, by a new time-resolved study.

Acknowledgments

JV acknowledges fruitful discussions with Michiel Sprik. Support from the Czech Science Foundation (grants 203/08/0114), the Czech Ministry of Education (grant LC512), and

the Academy of Sciences (Praemium Academie) is gratefully acknowledged. Part of the work in Prague was supported via Project Z40550506. OM acknowledges support from the International Max-Planck Research School for Dynamical Processes in Atoms, Molecules and Solids. Generous allocation of computer time from the Swiss National Supercomputer Centre (CSCS) is gratefully acknowledged. Experimental and theoretical work at the University of Southern California was supported by the U.S. National Science Foundation via CHE-0617060 and CHE-0957869 as well as the iOpenShell Center for Computational Studies of Electronic Structure and Spectroscopy of Open-Shell and Electronically Excited Species (CRIF:CRF CHE-0625419+0624602+0625237).

References

(1) B. C. Garrett, D. A. Dixon, D. M. Camaioni, D. M. Chipman, M. A. Johnson, C. D. Jonah, G. A. Kimmel, J. H. Miller, T. N. Rescigno, P. J. Rossky, S. S. Xantheas, S. D. Colson, A. H. Laufer, D. Ray, P. F. Barbara, D. M. Bartels, K. H. Becker, H. Bowen, S. E. Bradforth, I. Carmichael, J. V. Coe, L. R. Corrales, J. P. Cowin, M. Dupuis, K. B. Eisenthal, J. A. Franz, M. S. Gutowski, K. D. Jordan, B. D. Kay, J. A. LaVerne, S. V. Lymar, T. E. Madey, C. W. McCurdy, D. Meisel, S. Mukamel, A. R. Nilsson, T. M. Orlando, N. G. Petrik, S. M. Pimblott, J. R. Rustad, G. K. Schenter, S. J. Singer, A. Tokmakoff, L. S. Wang, C. Wittig, and T. S. Zwier, Chemical Reviews **105**, 355-389 (2005).

(2) G. V. Buxton, C. L. Greenstock, W. P. Helman, and A. B. Ross, Journal of Physical and Chemical Reference Data **17**, 513-886 (1988).

(3) P. Kambhampati, D. H. Son, T. W. Kee, and P. F. Barbara, Journal of Physical Chemistry A **106**, 2374-2378 (2002).

(4) J. A. Kloepfer, V. H. Vilchiz, V. A. Lenchenkov, X. Y. Chen, and S. E. Bradforth, Journal of Chemical Physics **117**, 766-778 (2002).

(5) G. Stein, Israel Journal of Chemistry **9**, 413-418 (1971).

(6) O. Marsalek, T. Frigato, J. VandeVondele, S. E. Bradforth, B. Schmidt, C. Schutte, and P. Jungwirth, Journal of Physical Chemistry B **114**, 915-920 (2010).

(7) K. H. Schmidt and D. M. Bartels, Chemical Physics **190**, 145-152 (1995).

(8) S. M. Pimblott, Journal of Physical Chemistry **95**, 6946-6951 (1991).

(9) T. Goulet and J.-P. Jay-Gerin, Journal of Chemical Physics **97**, 5076-5087 (1992).

(10) J. A. LaVerne, S. M. Pimblott, Journal of Physical Chemistry A **1)4**, 9820-9822 (2000).

(11) C. von Sonntag, *Free-Radical-Induced DNA Damage and Its Repair: A Chemical Perspective*. (Springer, Berlin, 2006).

(12) C. D. Jonah, D. M. Bartels, and A. C. Chernovitz, Radiation Physics and Chemistry **34**, 145-156 (1989).

(13) T. Ellenberger, *DNA Repair and Mutagenesis*. (ASM Press, Washington, D.C., 2005).

(14) Y. Gauduel, S. Pommeret, A. Migus, and A. Antonetti, Chemical Physics **149**, 1-10 (1990).

(15) B. Winter, R. Weber, W. Widdra, M. Dittmar, M. Faubel, and I. V. Hertel, Journal of Physical Chemistry A **108**, 2625-2632 (2004).

(16) C. G. Elles, A. E. Jailaubekov, R. A. Crowell, and S. E. Bradforth, Journal of Chemical Physics **125**, 044515 (2006).

(17) X. Chen, D. S. Larsen, S. E. Bradforth, and I. H. M. van Stokkum, Journal of Physical Chemistry A **115**, 3807-3819 (2011).

(18) P. Han and D. M. Bartels, Journal of Physical Chemistry **94**, 5824-5833 (1990).

(19) H. Tachikawa, Journal of Physical Chemistry A **106**, 6915-6921 (2002).

(20) P. A. Pieniazek, J. VandeVondele, P. Jungwirth, A. I. Krylov, and S. E. Bradforth, Journal of Physical Chemistry A **112**, 6159-6170 (2008).

(21) Q. Y. Cheng, F. A. Evangelista, A. C. Simmonett, Y. Yamaguchi, and H. F. Schaefer, Journal of Physical Chemistry A **113**, 13779-13789 (2009).

(22) G. H. Gardenier, M. A. Johnson, and A. B. McCoy, The Journal of Physical Chemistry A **113**, 4772-4779 (2009).

(23) E. Kamarchik, O. Kostko, J. M. Bowman, M. Ahmed, and A. I. Krylov, The Journal of Chemical Physics **132**, 194311-194311 (2010).

(24) H. Tachikawa, Journal of Physical Chemistry A **108**, 7853-7862 (2004).

(25) P. A. Pieniazek, E. J. Sundstrom, S. E. Bradforth, and A. I. Krylov, Journal of Physical Chemistry A **113**, 4423-4429 (2009).

(26) A. Furuhama, M. Dupuis, and K. Hirao, Physical Chemistry Chemical Physics **10**, 2033-2042 (2008).

(27) A. Furuhama, M. Dupuis, and K. Hirao, Journal of Chemical Physics **124**, 164310 (2006).

(28) C. G. Elles, I. A. Shkrob, R. A. Crowell, and S. E. Bradforth, Journal of Chemical Physics **126**, 164503 (2007).

(29) C. G. Elles, A. E. Jailaubekov, R. A. Crowell, and S. E. Bradforth, Journal of Chemical Physics **125**, 044515 (2006).

(30) P. A. Pieniazek, E. J. Sundstrom, S. E. Bradforth, and A. I. Krylov, Journal of Physical Chemistry A **113**, 4423–4429 (2009).

(31) C. G. Elles, C. A. Rivera, Y. Zhang, P. A. Pieniazek, and S. E. Bradforth, Journal of Chemical Physics **130**, 084501 (2009).

(32) A. Madarasz, P. J. Rossky, and L. Turi, Journal of Chemical Physics **126** (2007).

(33) D. Borgis, P. J. Rossky, and L. Turi, Journal of Chemical Physics **127** (2007).

(34) A. A. Mosyak, O. V. Prezhdo, and P. J. Rossky, Journal of Chemical Physics **109**, 6390-6395 (1998).

(35) G. B. Griffin, R. M. Young, O. T. Ehrler, and D. M. Neumark, Journal of Chemical Physics **131** (2009).

(36) A. E. Bragg, J. R. R. Verlet, A. Kammrath, O. Cheshnovsky, and D. M. Neumark, Science **306**, 669-671 (2004).

(37) A. R. Menzeleev and T. F. Miller, Journal of Chemical Physics **132**, - (2010).

(38) S. Grimme, Journal of Computational Chemistry **27**, 1787-1799 (2006).

(39) J. VandeVondele and M. Sprik, Physical Chemistry Chemical Physics **7**, 1363-1367 (2005).

(40) J. Heyd, G. E. Scuseria, and M. Ernzerhof, Journal of Chemical Physics **118**, 8207-8215 (2003).

(41) A. D. Becke, Journal of Chemical Physics **98**, 1372-1377 (1993).

(42) M. Sodupe, J. Bertran, L. Rodriguez-Santiago, and E. J. Baerends, Journal of Physical Chemistry A **103**, 166-170 (1999).

(43) D. M. Chipman, Journal of Physical Chemistry A **112**, 13372-13381 (2008).

(44) J. VandeVondele, M. Krack, F. Mohamed, M. Parrinello, T. Chassaing, and J. Hutter, Computer Physics Communications **167**, 103-128 (2005).

(45) H. J. C. Berendsen, J. R. Grigera, and T. P. Straatsma, Journal of Physical Chemistry **91**, 6269-6271 (1987).

(46) I. Janik, D. M. Bartels, and C. D. Jonah, Journal of Physical Chemistry A **111**, 1835-1843 (2007).

(47) Y. Shao, L. F. Molnar, Y. Jung, J. Kussmann, C. Ochsenfeld, S. T. Brown, A. T. B. Gilbert, L. V. Slipchenko, S. V. Levchenko, D. P. O'Neill, R. A. DiStasio, R. C. Lochan, T. Wang, G. J. O. Beran, N. A. Besley, J. M. Herbert, C. Y. Lin, T. Van Voorhis, S. H. Chien, A. Sodt, R. P. Steele, V. A. Rassolov, P. E. Maslen, P. P. Korambath, R. D. Adamson, B. Austin, J. Baker, E. F. C. Byrd, H. Dachsel, R. J. Doerksen, A. Dreuw, B. D. Dunietz, A. D. Dutoi, T. R. Furlani, S. R. Gwaltney, A. Heyden, S. Hirata, C. P. Hsu, G. Kedziora, R. Z. Khalliulin, P. Klunzinger, A. M. Lee, M. S. Lee, W. Liang, I. Lotan,

N. Nair, B. Peters, E. I. Proynov, P. A. Pieniazek, Y. M. Rhee, J. Ritchie, E. Rosta, C. D. Sherrill, A. C. Simmonett, J. E. Subotnik, H. L. Woodcock, W. Zhang, A. T. Bell, A. K. Chakraborty, D. M. Chipman, F. J. Keil, A. Warshel, W. J. Hehre, H. F. Schaefer, J. Kong, A. I. Krylov, P. M. W. Gill, and M. Head-Gordon, Physical Chemistry Chemical Physics **8**, 3172-3191 (2006).

(48) P. Hunt and M. Sprik, Chemphyschem **6**, 1805-1808 (2005).

(49) M. J. McGrath, J. I. Siepmann, I. F. W. Kuo, C. J. Mundy, J. VandeVondele, J. Hutter, F. Mohamed, and M. Krack, Journal of Physical Chemistry A **110**, 640-646 (2006).

(50) E. R. Davidson and W. T. Borden, Journal of Physical Chemistry **87**, 4783-4790 (1983).

(51) D. Marx, M. E. Tuckerman, J. Hutter, and M. Parrinello, Nature **397**, 601-604 (1999).

(52) P.M. Hare, E.A. Price and D.M. Bartels, Journal of Physical Chemistry A **112**, 6800-6802 (2008).

(53) V. H. Vilchiz, J. A. Kloepfer, A. C. Germaine, V. A. Lenchenkov, and S. E. Bradforth, Journal of Physical Chemistry A **105**, 1711-1723 (2001).

(54) M. K. Fischer, H. Rossmadl and H. Iglev, Journal of Chemical Physics **134**, 214507 (2011).

(55) A. E. Jailaubekov and S. E. Bradforth, Applied Physics Letters **87**, 021107 (2005).

(56) M. J. Tauber, R. Mathies, X. Chen, and S. E. Bradforth, Review of Scientific Instruments **74**, 4958-4960 (2003).

(57) R. Lian, R. A. Crowell, and I. A. Shkrob, Journal of Physical Chemistry A **109**, 1510-1520 (2005).

(58) V. H. Vilchiz, J. A. Kloepfer, A. C. Germaine, V. A. Lenchenkov, and S. E. Bradforth, Journal of Physical Chemistry A **105**, 1711-1723 (2001).

(59) D. M. Bartels and R. A. Crowell, Journal of Physical Chemistry A **104**, 3349-3355 (2000).

(60) Y. Zhang, L. Cass, C. G. Elles, and S. E. Bradforth, (unpublished).

(61) P. C. do Couto and D. M. Chipman, Journal of Chemical Physics **132**, 244307 (2010).

(62) E. Livshits, R. S. Granot, and R. Baer, Journal of Physical Chemistry A **115**, 5735-5744 (2011).

Table 1: Spin localization and proton hopping times in fs

	95 % localization	**first reactive proton hop**	**final reactive proton hop**
mean value	**31**	**33**	**77**
standard deviation	**21**	**14**	**45**

Figure captions:

Figure 1. Snapshots along a selected trajectory showing water molecules together with isosurfaces (at values of 0.01 and 0.001 au^{-3}) of the spin density. Panel a) shows the system right after ionization (t = 0) when the system is in the neutral geometry and the hole is partially delocalized. Panel b) depicts the system after the hole localizes almost entirely on a single water molecule, forming transient H_2O^+ (t = 40 fs). This species reacts almost instantaneously with a neighboring water molecule, forming an OH radical and a hydronium cation (highlighted in green), which eventually become separated by water molecules, as shown in Panel c) (t = 400 fs).

Figure 2. Maximum Mulliken spin population (as a measure of localization of the hole) on a single oxygen atom, shown as a function of time for all trajectories. The dashed line is at the value of 0.95, its intersection with each line marking the time when the localization is practically complete. DFT trajectories are depicted in blue, DFT-D trajectories in red. The black line is the average over all trajectories.

Figure 3. The distance between the center of spin and the center of charge, shown as a function of time for all the trajectories. This distance between an oxygen atom with the highest Mulliken spin population and that to which the excess proton is the closest monitors the progress of the proton transfer reaction. It is zero initially, becoming non-zero after the first proton hop. DFT trajectories are depicted in blue, DFT-D trajectories in red. The black line is the average over all trajectories.

Figure 4. Correlation between the time of localization and the time of reaction. The former is

defined as the time when the maximum Mulliken spin population on a single oxygen atom reaches 0.95 (dashed line in Figure 2). The latter is characterized by the reaction interval (depicted by a line) that starts at the moment of the first proton transfer (full circles) and ends when no more back transfer to the original hole occurs (open circles). DFT trajectories are depicted in blue, DFT-D trajectories in red. The full line shows direct proportion between the two times for reference.

Figure 5. Correlations between the distance between the oxygen atoms involved in the proton transfer reaction and the distance between the transferring hydrogen atom and its new oxygen bonidng partner along all simulated trajectories. Blue circles mark the initial conditions and blue lines denote the trajectory segments until the reaction starts. Red segments with red circles at their boundaries mark the reaction intervals (as defined in Figure 4). Gray segments show the rest of the trajectories after the reaction.

Figure 6. Snapshots of the aqueous bulk system right after ionization (t= 0) for a selected trajectory using different electronic structure methods. Water molecules are shown together with isosurfaces of the spin density.

Figure 7. Water pentamer as a benchmark cluster system, calculated with different methods (see text for detail). Water molecules are shown together with isosurfaces of the spin density.

Figure 8. (a) Time evolution of electronic excitation spectrum for ionized bulk water. Average of 18 AIMD trajectories with excitations computed for core trimer at the EOM-IP-CCSD level (see text). Stick spectra for each trajectory are broadened with 0.6 eV FWHM Gaussian. Excitations shown only for 1 – 5 eV, the optically accessible range. (b) As panel (a) except the that the computed spectral intensity is turned on for each trajectory only when the spin is 95%

localized as judged by analysis of the BLYP-SIC density, see Figure 4. Intensity scale bar in both plots is the oscillator strength density relative to that of the corresponding gas phase OH radical transition (0.00312).

Figure 9. Comparing spectral predictions and experiment. (A and C) Experimental transient absorption spectra with a continuum probe and time resolution of 40-50 fs. Photoionization of pure liquid water achieved with 2 photons giving a total excitation energy ~ 11 eV. Scale bar is transient absorbance in mOD. The signal aligned along zero delay is coherent pump+probe absorption and is observed in absence of ionization (see text). In panel A, cross phase modulation between the pump and 800 nm driven probe continua is observed (see arrow) – this is minimized by driving the continuum at 1350 nm, panel C. Signal rising to maximum at 500 fs delay most prominently at 700 nm is from the solvated electron; when fully developed, the absorbance at 720 nm is 20 mOD. (B and D) Simulated spectrum for ground state cationic hole in bulk water, reproduced from Figure 8(b) but now shown matching experimental range of probe wavelengths and normalized to peak spectral intensity. Recall the spectral simulation shows only signals attributable to the ionized and localized hole. These signals are not apparent in the experimental datasets.

Figure 10. Spectral cuts from the four panels of Figure 9 at four pump-probe delays comparing theoretical prediction (B and D) and experimental reality (A and C). No blue shifting feature is picked up experimentally.

Figure 1:

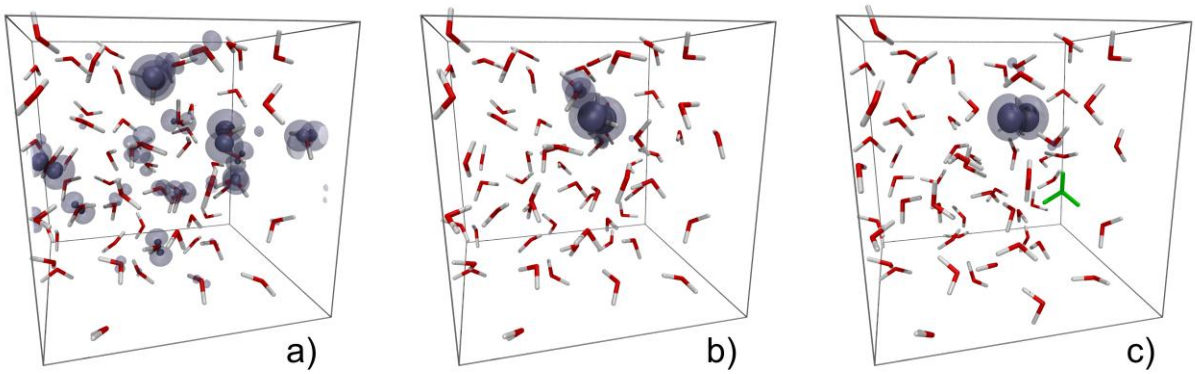

Figure 2:

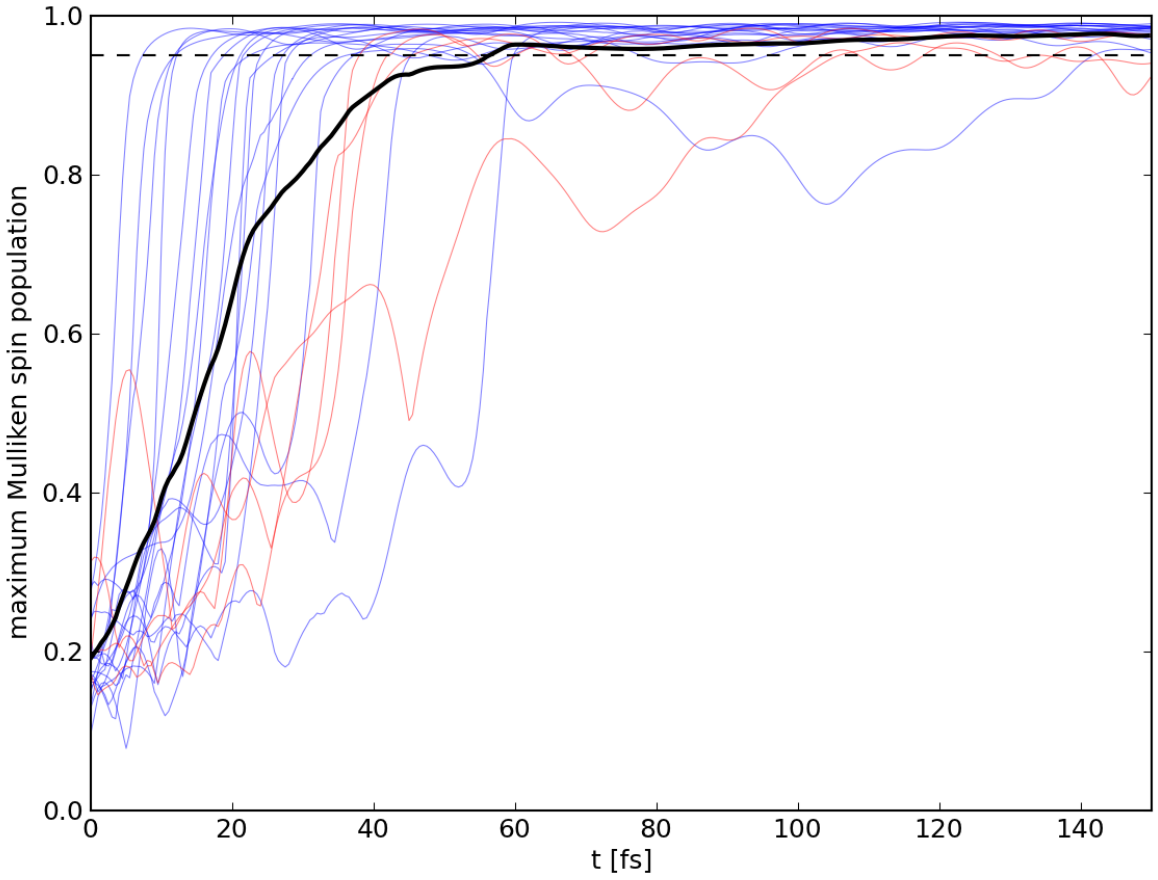
maximum Mulliken spin population
t [fs]
0.0
0.2
0.4
0.6
0.8
1.0
0
20
40
60
80
100
120
140

Figure 3:

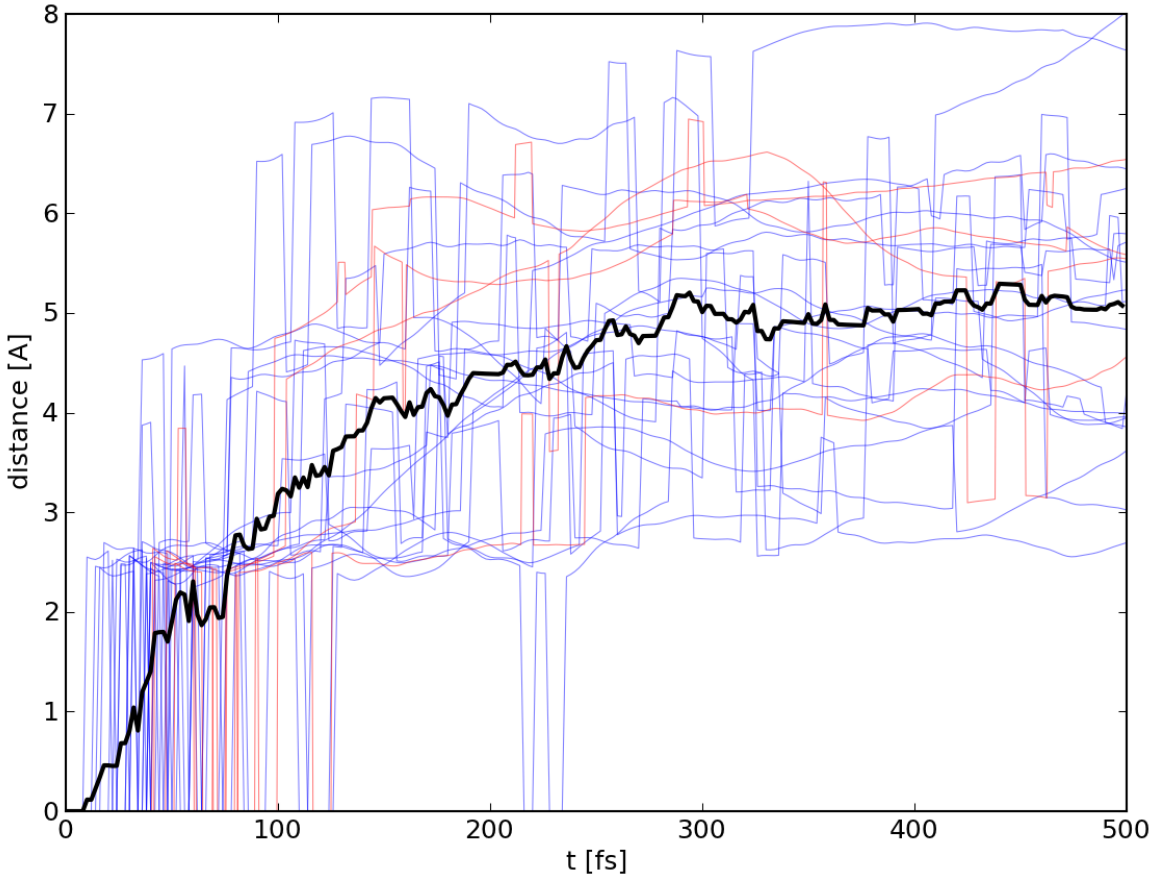

Figure 4:

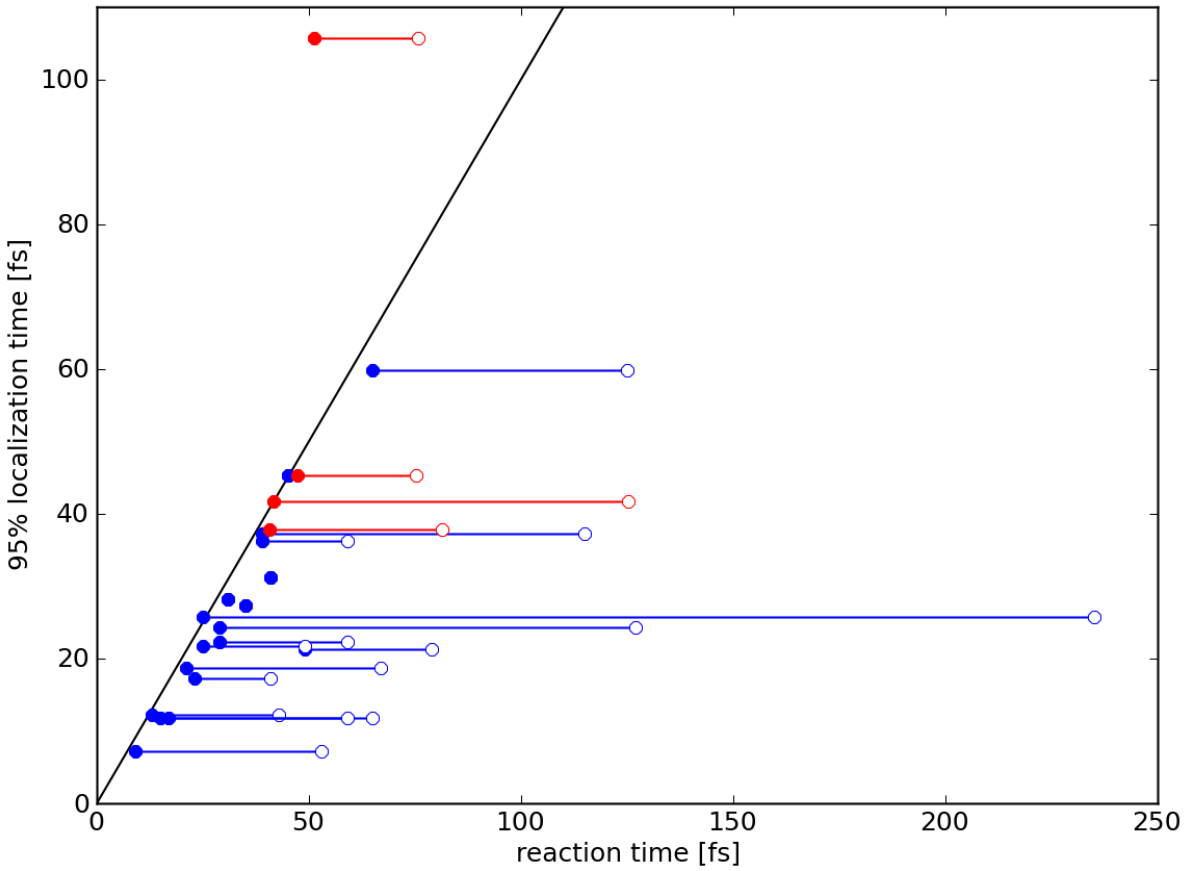
95% localization time [fs]
reaction time [fs]
0
20
40
60
80
100
0
50
100
150
200
250

Figure 5:

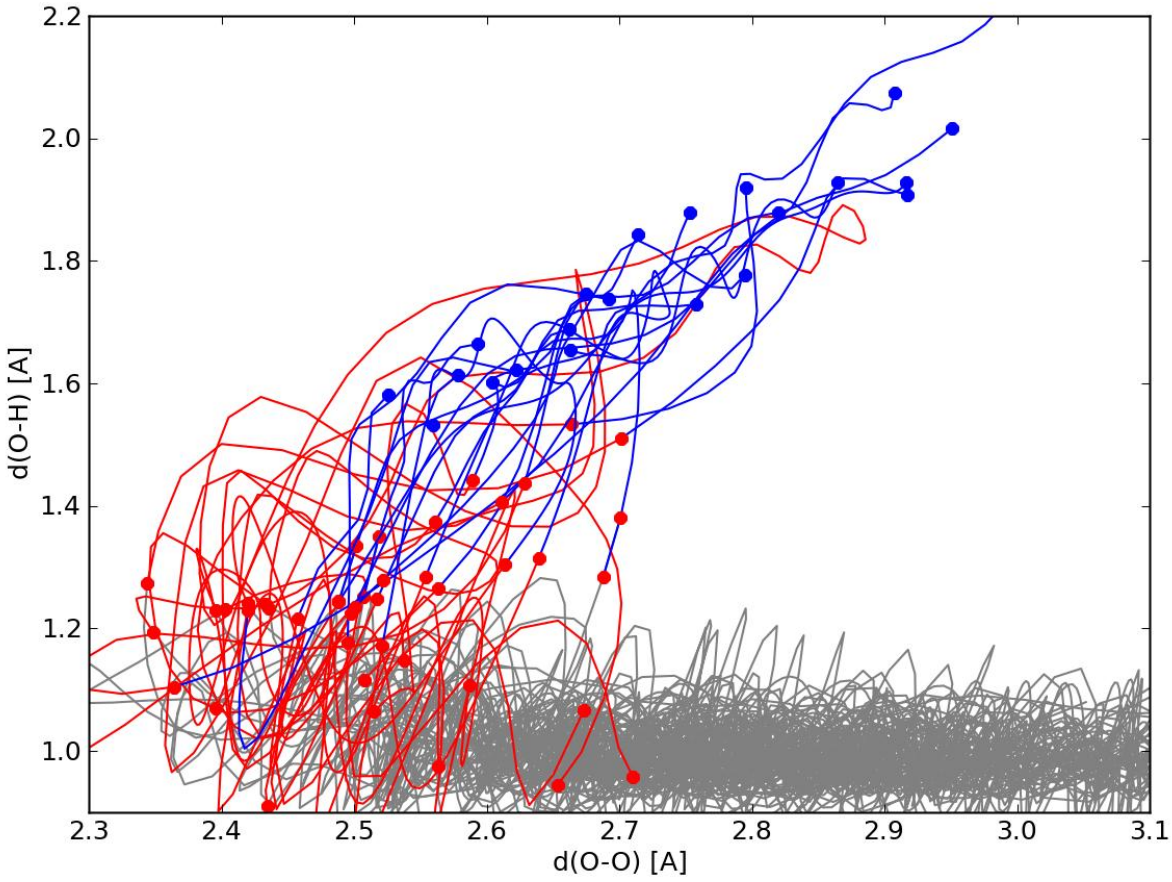

Figure 6:

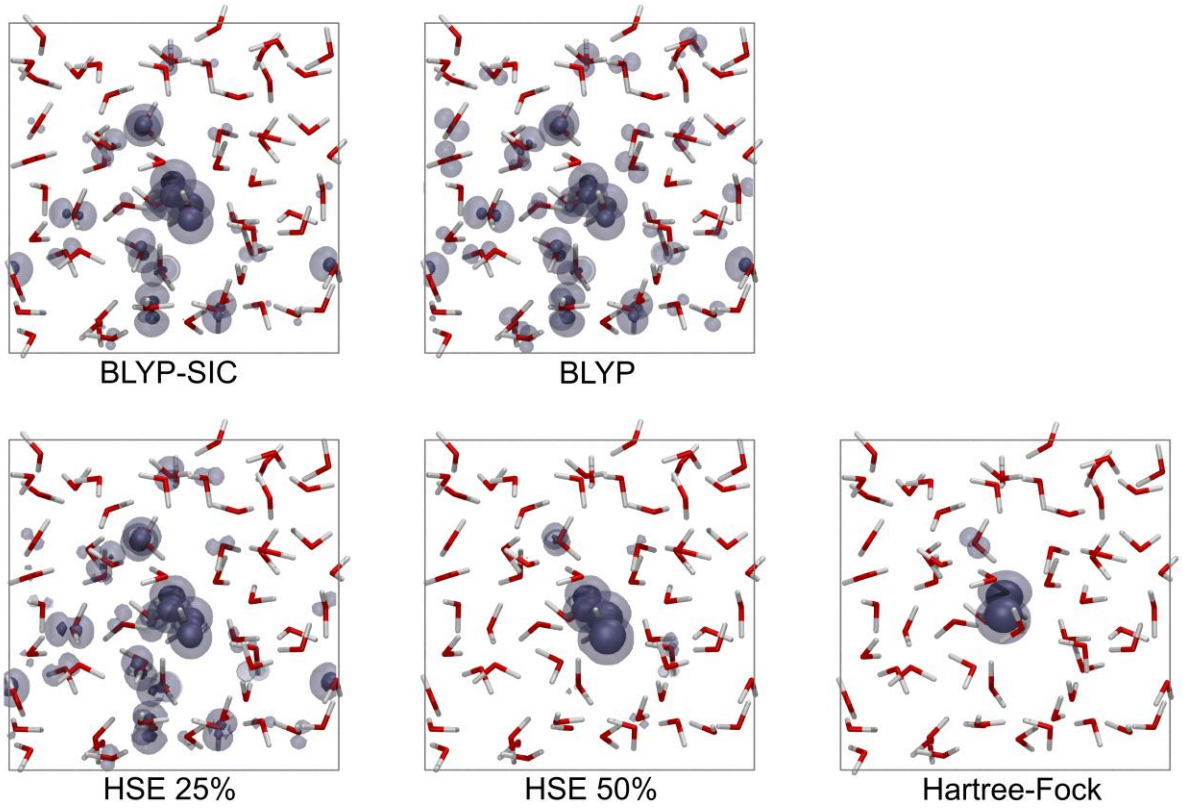

Figure 7:

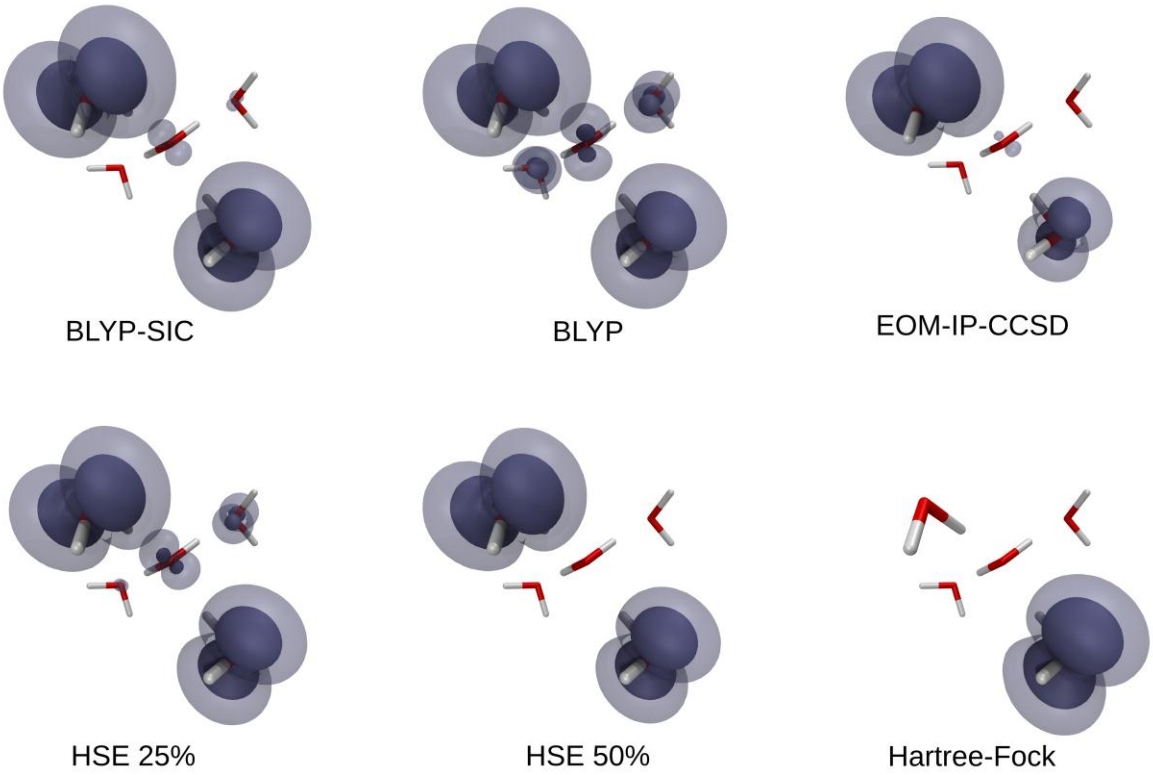

Figure 8 (a):

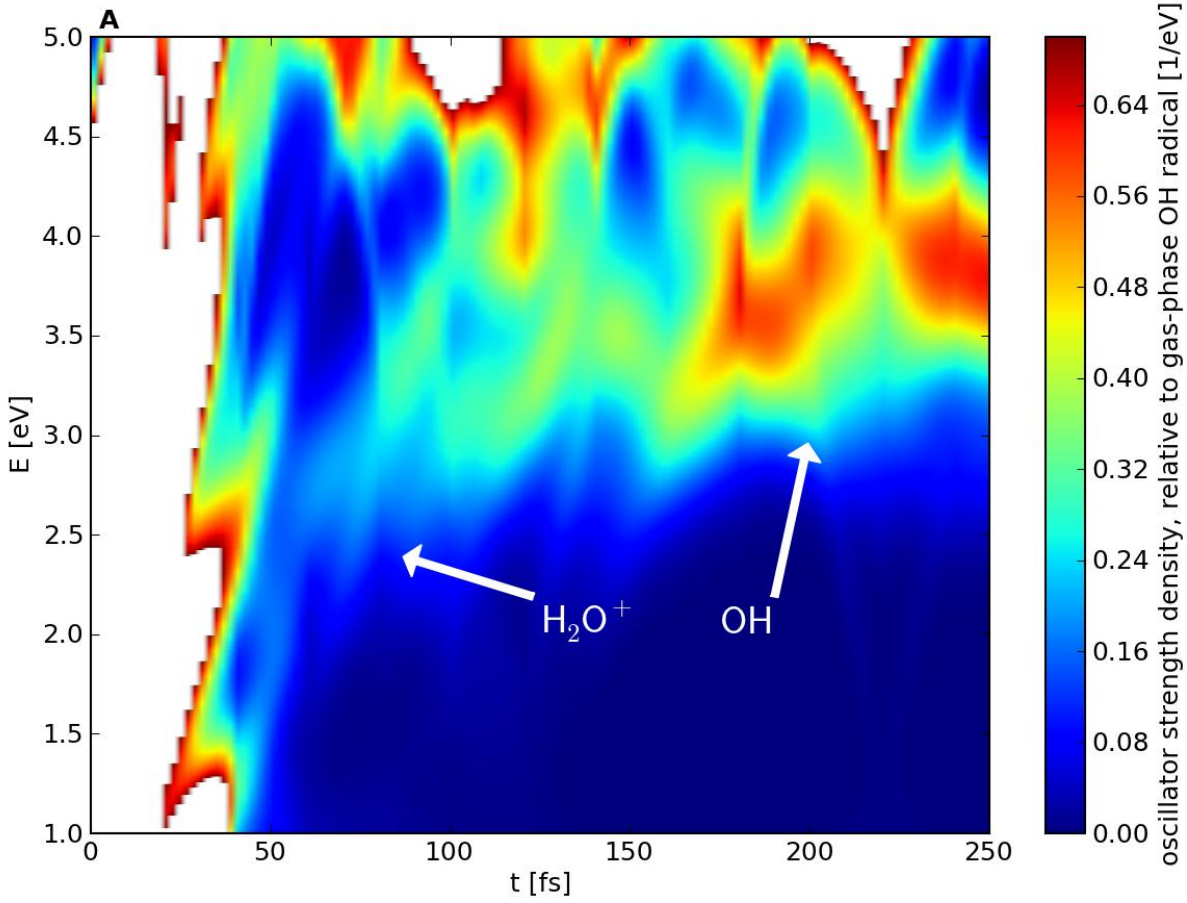
A
E [eV]
t [fs]
H_2O^+
OH
oscillator strength density, relative to gas-phase OH radical [1/eV]

Figure 8(b):

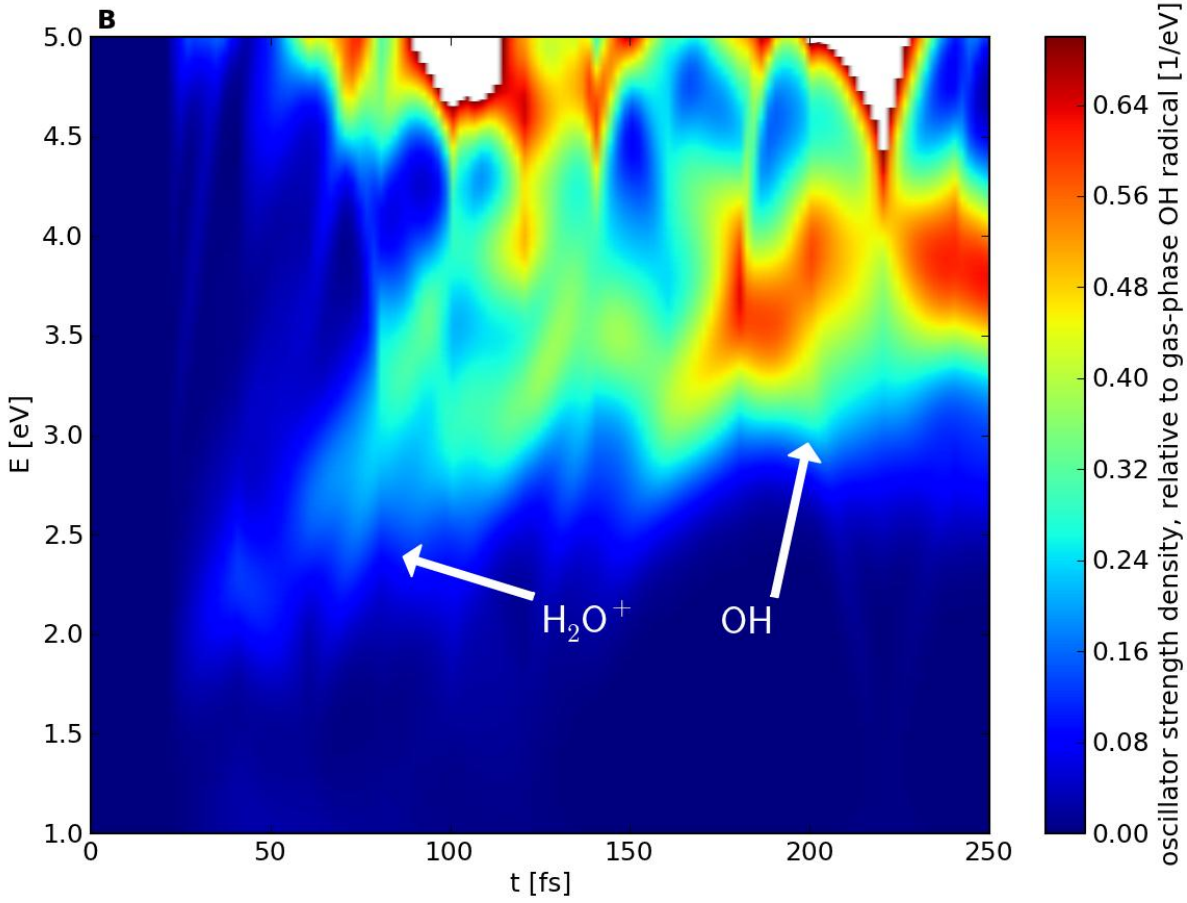
B
5.0
4.5
4.0
3.5
3.0
2.5
2.0
1.5
1.0
E [eV]
0
50
100
150
200
250
t [fs]
H_2O^+
OH
0.64
0.56
0.48
0.40
0.32
0.24
0.16
0.08
0.00
oscillator strength density, relative to gas-phase OH radical [1/eV]

Figure 9:

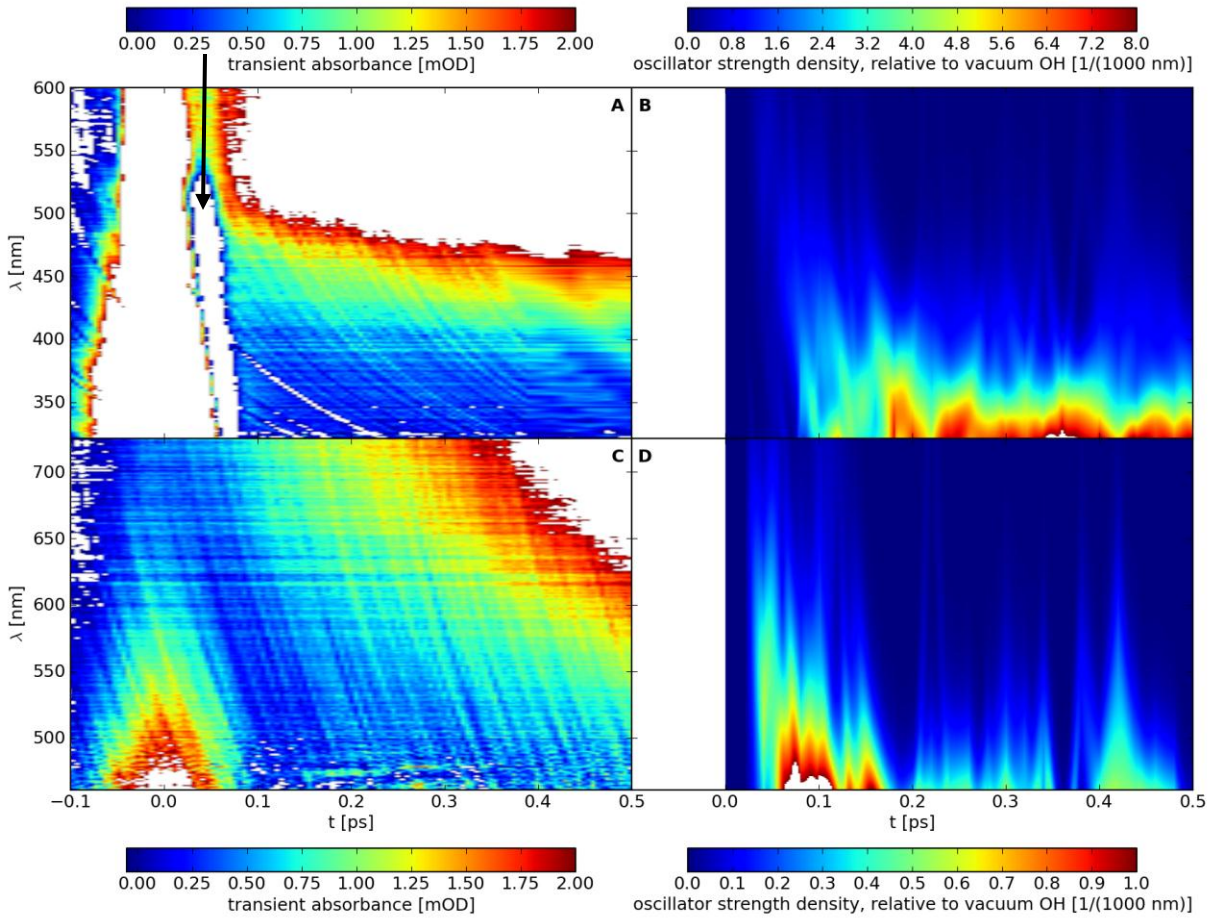
0.00 0.25 0.50 0.75 1.00 1.25 1.50 1.75 2.00
transient absorbance [mOD]
0.0 0.8 1.6 2.4 3.2 4.0 4.8 5.6 6.4 7.2 8.0
oscillator strength density, relative to vacuum OH [1/(1000 nm)]
A
B
C
D
λ [nm]
600
550
500
450
400
350
700
650
600
550
500
−0.1 0.0 0.1 0.2 0.3 0.4 0.5
t [ps]
0.0 0.1 0.2 0.3 0.4 0.5
t [ps]
0.00 0.25 0.50 0.75 1.00 1.25 1.50 1.75 2.00
transient absorbance [mOD]
0.0 0.1 0.2 0.3 0.4 0.5 0.6 0.7 0.8 0.9 1.0
oscillator strength density, relative to vacuum OH [1/(1000 nm)]

Figure 10:

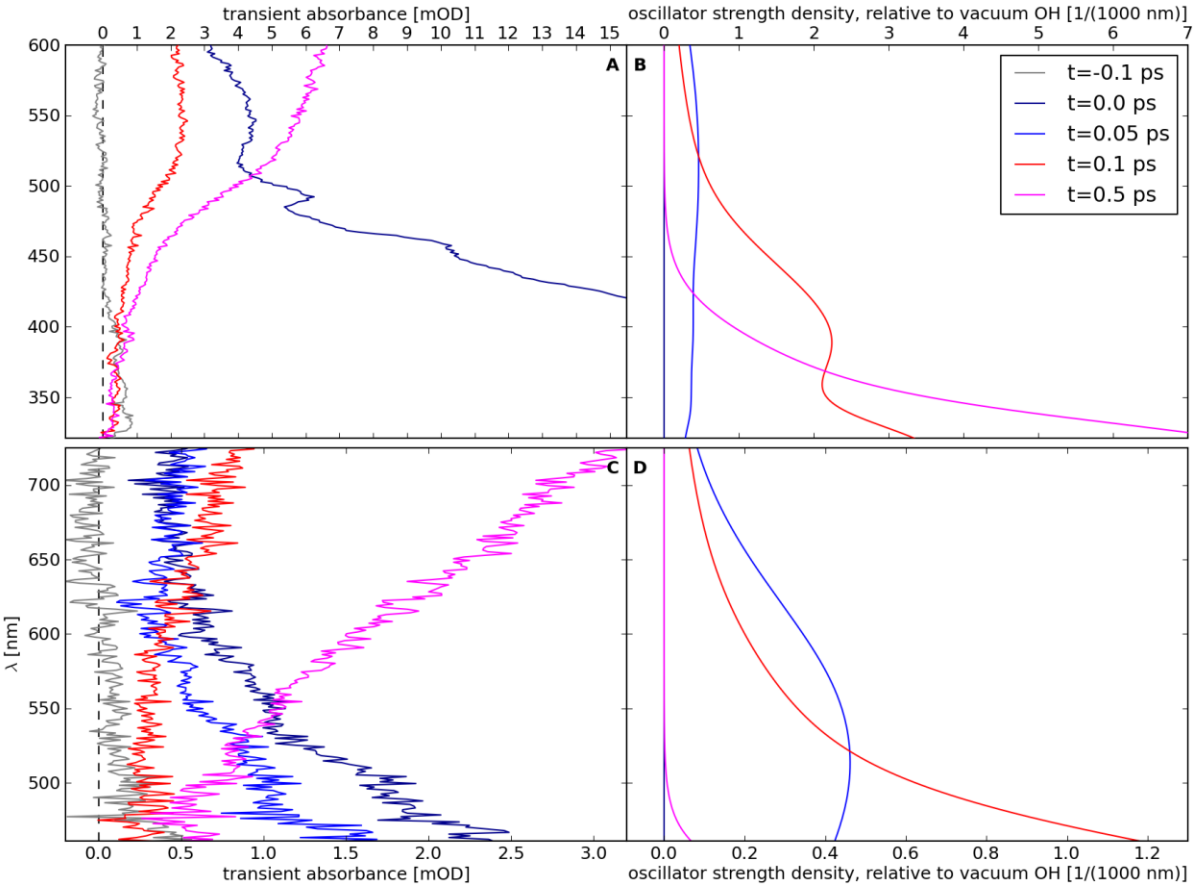
transient absorbance [mOD]
oscillator strength density, relative to vacuum OH [1/(1000 nm)]
A
B
C
D
t=-0.1 ps
t=0.0 ps
t=0.05 ps
t=0.1 ps
t=0.5 ps
λ [nm]
transient absorbance [mOD]
oscillator strength density, relative to vacuum OH [1/(1000 nm)]

TOC

Partially delocalized spin density in water right after ionization.